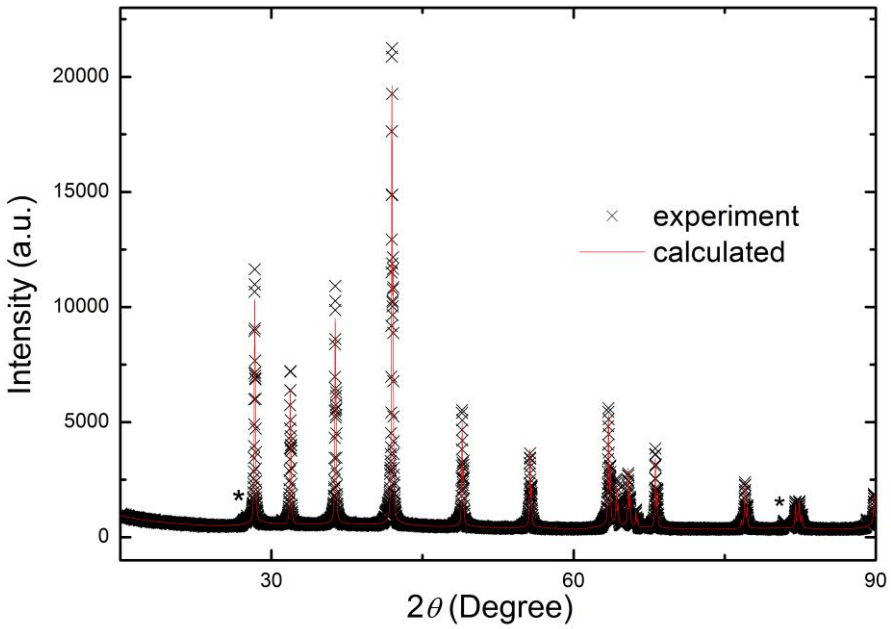

Supplementary Figure 1 | The x-ray diffraction pattern of pristine TaP at ambient pressure. The red line is the Rietveld refinement result of TaP with space group $I4_1md$. Two tiny peaks marked with asterisk (*) come from the instrument background.

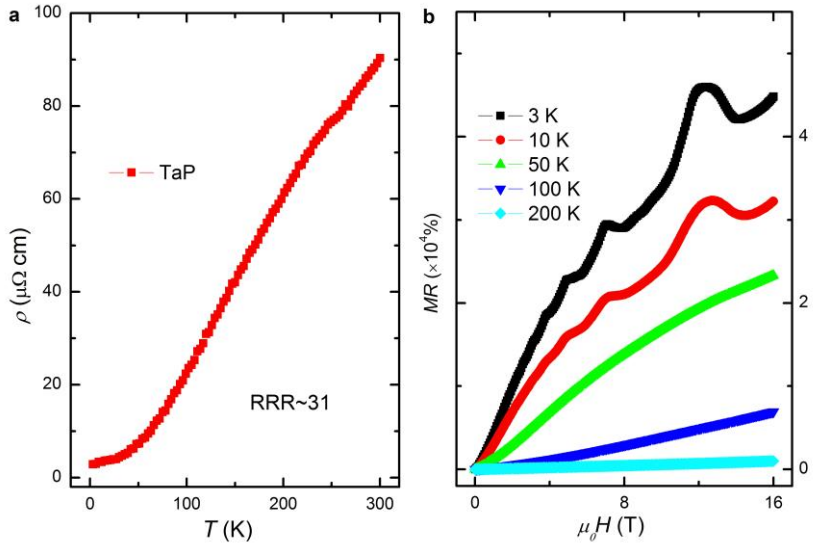

Supplementary Figure 2 | Resistivity and MR of TaP single crystals. (**a**)

Temperature dependent resistivity under ambient pressure of TaP. (**b**) MR data at different temperatures with external magnetic field paralleled to c-axis. The SdH oscillations appear on the MR curve at 3 K (black) and 10 K (red).

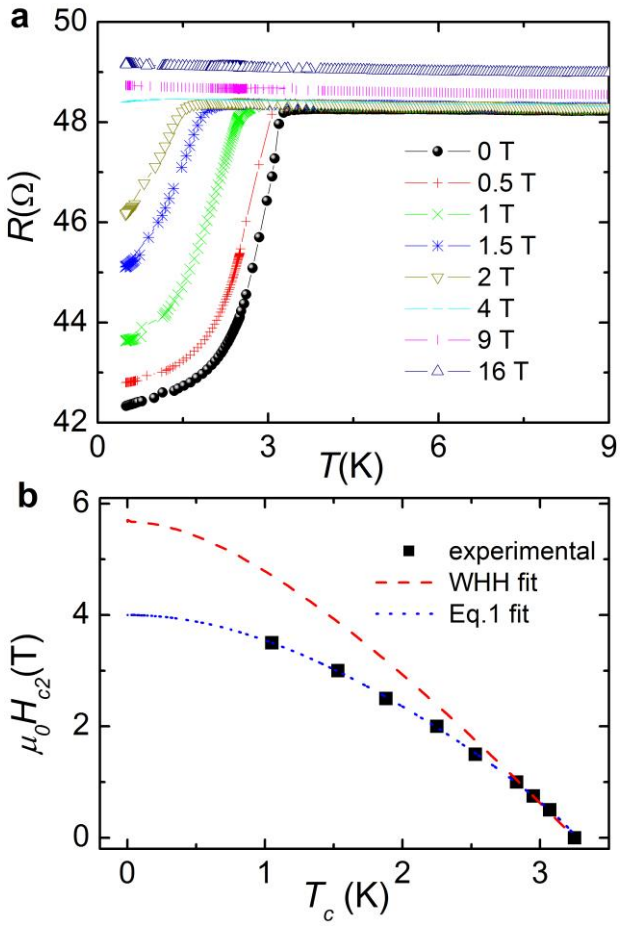

Supplementary Figure 3 | Temperature dependence of resistance and upper critical field measured from the pressure released sample. (a) *R(T)* curves under fields up to 16 T. The superconducting transition is totally suppressed above 0.4 K at 4 T. (b) The upper critical field $\mu_0 H_{c2}$ versus *T* shown by the black squares. The red dashed line is the WHH fitting curve and the blue dotted line is the fitting result of Supplementary Equation 1.

Supplementary Table 1 | The coordinates (in units of the length of Γ−Σ for x and y, and of the length of Γ-Z for z) and energies (in meV) of W2 at pressure of 0 GPa to 30 GPa. The energy values are relative to the Fermi level.

	x	y	z	E-W2(meV)
0 GPa	0.031	0.505	0.583	15.0
10 GPa	0.031	0.504	0.568	5.1
20 GPa	0.030	0.503	0.553	-0.62
30 GPa	0.030	0.501	0.541	-21.4

Supplementary Note 1 | Evolution of the structure and the Weyl point positions with pressure

Calculated coordinates and energies of W2 under pressures from 0 GPa to 30 GPa are listed in Supplementary Table 1. Other W2 points are related to the W2 point in Supplementary Table 1 by mirror symmetry, C_4 rotation and time-reversal symmetry. And all the energies of W2 points are equal. The coordinates of W2 at 0 GPa are consistent with previous work[1]. With the increase of pressure, the coordinate x and y of W2 are basically maintained while the coordinate z of W2 decreases from 0.585 to 0.541. It is surprising that the energies of W2 relative to Fermi level change significantly with the increase of pressure.

Supplementary Note 2 | Measurements and determination of $\mu_0 H_{c2}$ in TaP after decompression from 100 GPa

Since superconductivity survives after the decompression, we thus did a new round of pressurizing experiment at room temperature. We chose a fresh TaP

sample and ramped the pressure up to 100 GPa, kept it for 24 hours and then released the pressure to 1 bar. Afterwards, we put electrode contacts to measure the resistivity from room temperature to 0.3 K. Since the sample has only a size of about 30 μm after being successfully exfoliated from the diamond anvil cell, we only managed to make two electrodes instead of four on the sample with an irregular shape, the contacting resistance is still included. Without pressure cell, we were able to measure the resistivity down to He^3 temperature (T = 0.3 K) with magnetic fields up to 16 T, and the results are shown in Supplementary Fig. 3a. One can clearly see the superconducting transition starting at about 3.25 K. The superconducting transition shifts gradually down to lower temperatures with increasing magnetic field and the transition temperature is totally suppressed to below 0.3 K when magnetic field exceeds 4 T. A positive and moderate MR effect can be observed from these measurements. In addition, we determine the upper critical field $\mu_0 H_{c2}$(T) by using the standard crossing method, which determines the superconducting transition temperature by the crossing point of extrapolating lines of the normal state and the steep transition part. In Supplementary Fig. 3b we plot the $\mu_0 H_{c2}$ versus T by using filled symbols, and the fitting result by the Werthamer-Helfand-Hobenberg (WHH) formula is shown in red dashed line. The experimental data slightly deviate from the WHH formula at high magnetic fields. The blue dotted curve is the fitting result with following equation

$$H_{c2}(T) = H_{c2}(0)\frac{[1-(T/T_c)^2]^{\alpha}}{[1+(T/T_c)^2]^{\beta}}. \quad \text{(S1)}$$

We adopt this expression with two terms of $1-(T/T_c)^2$ and $1+(T/T_c)^2$ as components because they are the basic ingredients for the description of critical fields. The obtained $\mu_0 H_{c2}(0)$ is about 4 T.

Supplementary Note 3 | XRD characterization and magnetoresistance of pristine TaP

The XRD data were collected on TaP powders by crushing and grinding the as prepared TaP single crystals. The XRD and the Rietveld refinement result with weighted profile R-factor R_{wp} = 8.789% are shown in Supplementary Fig. 1. The refined cell parameters are a = 3.320 Å and c = 11.343 Å. Two tiny peaks that cannot be indexed with TaP come from the instrument background. The rather clean XRD data indicate the high purity of the sample.

Temperature dependent resistivity of a TaP single crystal under ambient pressure is shown in Supplementary Fig. 2a. The residual resistivity ratio (RRR) (comparing the *R*(300 K) to the lowest temperature value at 3 K) reaches 31. MR of the pristine TaP single crystal are shown in Supplementary Fig. 2b with magnetic fields up to 16 T at temperatures 3 K, 10 K, 50 K, 100 K and 200 K. Shubnikov-de Haas (SdH) oscillations are clearly shown at 3 K and 10 K. A maximum value of MR about 45000% was observed at 3 K and 16 T.

Supplementary Note 4 | Resistivity measurements under high pressures

High-pressure resistance measurements with different warming-cooling cycles were conducted with the four probe method in a screw-pressure-type diamond anvil cell (DAC). Platinum (Pt) foils with a thickness of 2 μm were used as electrodes. Diamond anvils of 200μm–culets and rhenium gasket covered with a mixture of epoxy and fine cubic boron nitride (c-BN) powder were used here. A single crystal with typical dimension of 65×20×5 μm^3 was loaded without pressure-transmitting medium. Pressure was calibrated by using the ruby fluorescence scale below 70 GPa[2] and the diamond Raman scale above 70 GPa[3].

Supplementary Note 5 | High-pressure x-ray diffraction measurements

The angle-dispersive XRD experiments under high pressure were performed at the HPCAT beamline 16-BM-D at the Advanced Photon Source, Argonne National Laboratory. A MAR345 image plate detector was equipped in the beamline and the diffraction was processed in a transmission mode. The energy of x-ray for the experiments was set to 33.169 keV. The application of high pressure was realized with a pair of 100μm-culet diamonds mounted on a symmetric diamond anvil cell. A 301 stainless steel sheet was used as a gasket and silicone oil as a pressure-transmitting medium. The pressure-transmitting medium was sealed in a 50μm-diameter hole pre-drilled on the gasket for preserving a quasi-hydrostatic pressure environment to the TaP sample. The drilling was done using a laser micro-machining system developed by HPCAT[4].

Supplementary Note 6 | Ab initial calculations

Ab initio random searching (AIRSS) method[5-6] was applied for crystal structure predictions in the frame of density-functional theory (DFT). Enthalpy and band structure calculations were performed with the projected augmented wave (PAW) method implemented in the Vienna ab initio simulation package code (VASP)[7-9] with Perdew-Burke-Ernzerhof (PBE)[10] generalized gradient approximation (GGA) exchange-correlation functional. The cutoff energy of 400 eV was set for a plane wave basis. The calculations of phonon spectrum were performed in a $3 \times 3 \times 2$ supercell being computed with the PHONOPY code[11] and VASP code.

The calculations of semi-classic transport conductivity were performed using Boltzmann equation method implemented in the BoltzTraP package[12-13], and the mesh for self-consistent band energies is 16x16x22. Spin-orbit coupling was concerned during calculations. The maximally localized Wannier functions (WLWF)[14] for the d orbitals of Ta atoms and p orbitals of P atoms were constructed. The projected surface states were calculated using surface Green's function in the semi-infinite system[15, 16].

Supplementary References

1. Weng, H., Fang, C., Fang, Z., Bernevig, B. A., & Dai, X. Weyl semimetal phase in noncentrosymmetric transition-metal monophosphides. *Phys. Rev. X* **5**, 011029 (2015).

2. Mao, H. K., Xu, J. A., & Bell, P. M. Calibration of the ruby pressure gauge to 800 kbar under quasi-hydrostatic conditions. *J. Geophys. Res.* **91**, 4673 (1986).
3. Akahama, Y., & Kawamura, H. High-pressure Raman spectroscopy of diamond anvils to 250 GPa: Method for pressure determination in the multimegabar pressure range. *J. Appl. Phys.* **96**, 3748 (2004).
4. Hrubiak, R., Sinogeikin, S., Rod, E., & Shen, G. The laser micro-machining system for diamond anvil cell experiments and general precision machining applications at the High Pressure Collaborative Access Team. *Rev. Sci. Instrum.* **86**, 072202 (2015).
5. Pickard, C. J., & Needs, R. J. High-pressure phases of silane. *Phys. Rev. Lett*. **97**, 045504 (2006).
6. Pickard, C. J., & Needs, R. J. Ab initio random structure searching. *J. Phys.: Condens. Matter* **23**, 053201 (2011).
7. Kresse, G., & Joubert, D. From ultrasoft pseudopotentials to the projector augmented-wave method. *Phys. Rev. B* **59**, 1758 (1999).
8. Kresse, G., & Furthmüller, J. Efficient iterative schemes for ab initio total-energy calculations using a plane-wave basis set. *Phys. Rev. B* **54**, 11169 (1996).
9. Kresse, G., & Furthmüller, J. Efficiency of ab-initio total energy calculations for metals and semiconductors using a plane-wave basis set. *Comput. Mater. Sci*. **6**, 15-50 (1996).

10. Perdew, J. P., Burke, K., & Ernzerhof, M. Generalized gradient approximation made simple. *Phys. Rev. Lett.* **77**, 3865 (1996).
11. Togo, A., Oba, F., & Tanaka, I. First-principles calculations of the ferroelastic transition between rutile-type and CaCl 2-type SiO 2 at high pressures. *Phys. Rev. B* **78**, 134106 (2008).
12. Madsen, G. K., & Singh, D. J. BoltzTraP. A code for calculating band-structure dependent quantities. *Comput. Phys. Commun.* **175**, 67 (2006).
13. Kuneš, J., Novak, P., Schmid, R., Blaha, P., & Schwarz, K. Electronic structure of fcc Th: Spin-orbit calculation with 6 p 1/2 local orbital extension. *Phys. Rev. B* **64**, 153102 (2001).
14. A. A. Mostofi, J. R. Yates, Y. S. Lee, I. Souza, D. Vanderbilt, and N. Marzari, *Comput. Phys. Commun.* **185**, 2309 (2014).
15. Sancho, M. L., Sancho, J. L., & Rubio, J. Quick iterative scheme for the calculation of transfer matrices: application to Mo (100). *J. Phys. F* **14**, 1205 (1984).
16. Sancho, M. L., Sancho, J. L., Sancho, J. L., & Rubio, J. Highly convergent schemes for the calculation of bulk and surface Green functions. *J. Phys. F.* **15**, 851 (1985).